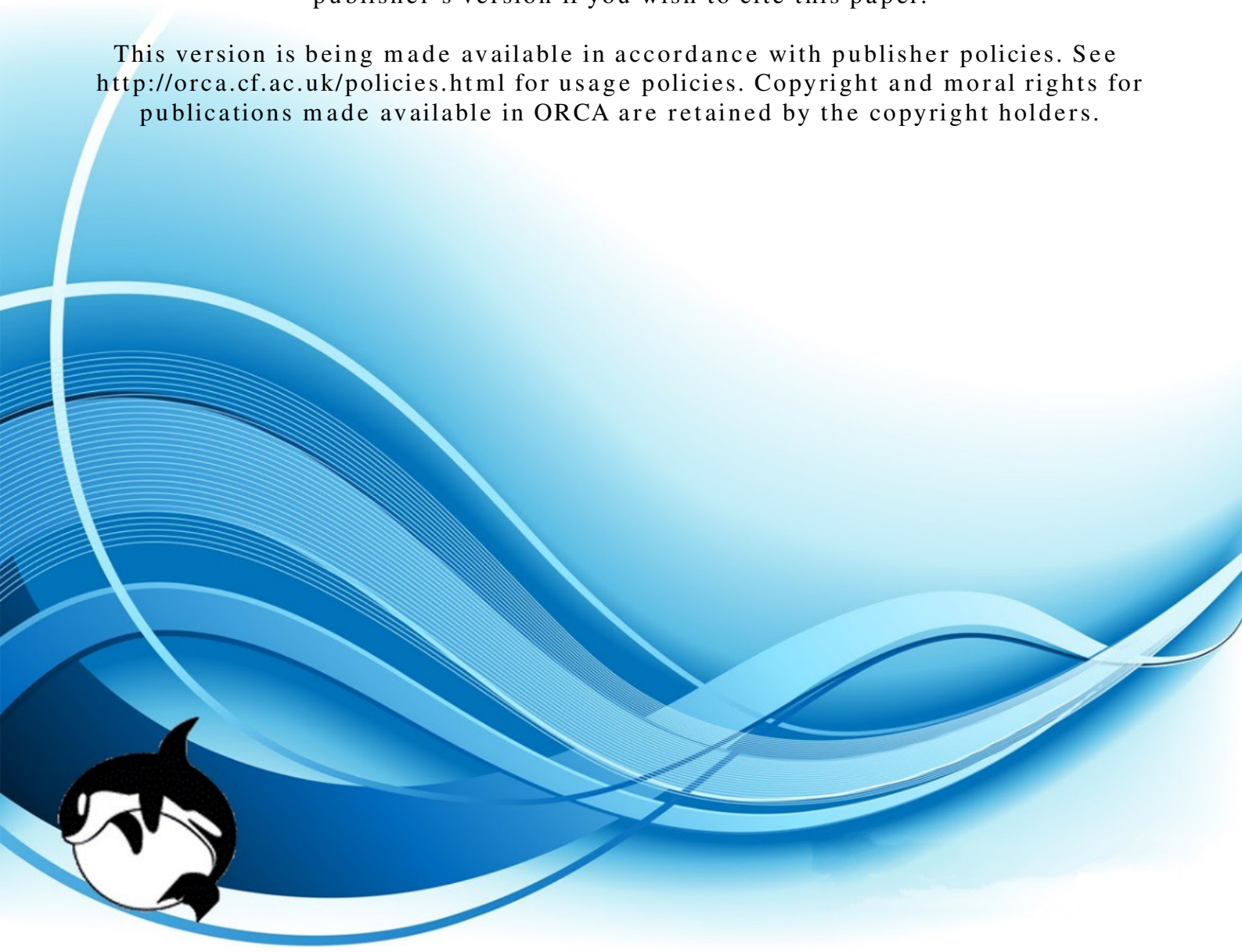

Orientation and Anisotropy of Multi Component Shapes from Boundary Information

Paul L. Rosin,* Joviša Žunić†

Abstract

We define a method for computing the orientation of compound shapes based on boundary information. The orientation of a given compound shape S is taken as the direction α that maximises the integral of the squared length of projections, of all the straight line segments whose end points belong to particular boundaries of components of S to a line that has the slope α. Just as the concept of orientation can be extended from single component shapes to multiple components, elongation can also be applied to multiple components, and we will see that it effectively produces a measure of anisotropy since it is maximised when all components are aligned in the same direction. The presented method enables a closed formula for an easy computation of both orientation and anisotropy.

Keywords: Shape, compound shape, orientation, anisotropy, image processing, early vision.

*School of Computer Science, Cardiff University, Cardiff CF24 3AA, Wales, U.K. e-mail: Paul.Rosin@cs.cf.ac.uk

†Department of Computer Science, University of Exeter, Exeter EX4 4QF, U.K. e-mail: J.Zunic@ex.ac.uk J. Žunić is also with the Mathematical Institute, Serbian Academy of Arts and Sciences, Belgrade.

1 Introduction

1.1 Region Boundary versus Region Interior

A distinction is sometimes made between methods for shape analysis that operate on a region's interior (i.e. the enclosed area) as opposed to those that process the exterior (i.e. its boundary) [23] – in this paper we are considering only region masks and ignoring interior intensities or colours. The interior can be reconstructed from the exterior, and vice-versa, and so the two representations are equivalent in the information they contain. Nevertheless, the distinction remains since that methods that operate on the interior often tend to be dominated by the global properties of the shape, whereas boundary-based methods are often more sensitive to local properties. This is made clear by using as a concrete example two standard methods for measuring the convexity of a shape S using its convex hull $CH(S)$. The interior based method uses areas and define the convexity measure $\mathcal{C}_1(S)$, of a given shape S, as: $\mathcal{C}_1(S) = \frac{Area(S)}{Area(CH(S))}$, while the boundary-based method uses perimeters for an alternative definition of the shape convexity: $\mathcal{C}_2(S) = \frac{Perimeter(CH(S))}{Perimeter(S)}$. Substantial differences in the approaches can be seen on many shapes, one example being shown in figure 1. The overall shape is a (convex) rectangle, and since the indentations are relatively thin their area is small. Consequently according to $\mathcal{C}_1(S)$ this shape has a high degree of convexity. On the other hand, it would receive a low convexity score from $\mathcal{C}_2(S)$ since the boundary has many deviations from the convex hull.

The majority of methods used in shape analysis and shape classification are area based ones. A reason for this is their robustness, which is particularly an advantage when working with low quality data. Another reason could be that such methods are assumed to be easier

Figure 1: A shape with deep but narrow indentations which is considered highly convex by $\mathcal{C}_1$ but not by $\mathcal{C}_2$.

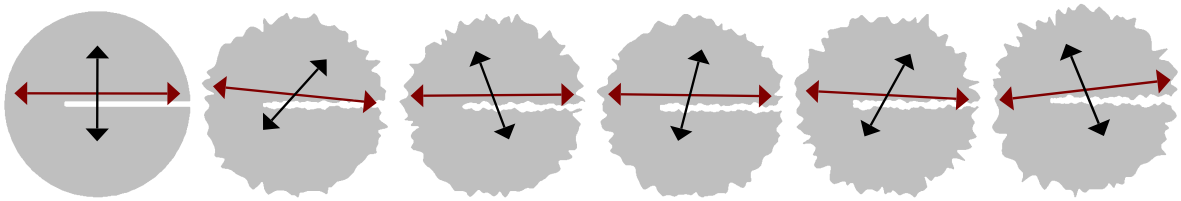

Figure 2: Orientations of a noisy indented circle computed using the (standard) interior based moments (shown as the short black arrows) and boundary-based moments (shown as the longer arrows).

to analyse and to develop. For example, consider the basic problem of computing the size of a shape. When its area is used, it is often sufficient to enumerate the number of pixels inside the studied shape, multiply this number with the pixel size and this is (in many applications) a reasonably good estimate for the shape's size. An analogous discussion holds when working with shape moments and moment invariants – it is, again, relatively easy to get good approximations of real moments (moment invariants) by applying simple operations on the set of pixels inside the shape [17]. In contrast, consider using a boundary based measure of a shape's size such as perimeter. When working in a discrete (digital) space, computing perimeter is well known to be a very difficult task [4, 30].

Recently, despite the difficulties when working with boundary information in a discrete space, there is ongoing interest in methods and tools that could extract information from shape boundaries. Such an interest is due to a strong demand for powerful tools in, for example, object and person identification, but also in many other computer vision and image processing application. We cite just a few recent works [2, 7, 13, 20, 21, 26, 28, 29] for an illustration.

In this paper we shall also describe a method for analysing shape by boundaries or contours. The method will involve computation of line-based moments instead of the area based ones. Line-based moments provide more sensitivity to boundary detail; of course, depending on the application this sensitivity can be considered either as an advantage (providing extra discriminatory power) or a disadvantage (oversensitivity to noise). Another aspect of using line-based moments – which can generally be seen as an advantage – is that they can be easily and directly applied to objects that are intrinsically linear rather than regional (e.g. edges, signatures, etc.), even if the boundaries are open or fragmented.

Specifically, this paper will address the issue of determining the orientation of shapes.

Figure 2 provides an example demonstrating in this context the difference between interior and boundary-based methods. In both cases the standard formula using moments was used. The shape in figure 2 is basically a circle, which is not orientable using the area-based moments method [38]. However, the circle contains a deep intrusion, giving it a perceptually well defined orientation. Nevertheless, since the intrusion is relatively narrow, and therefore has a small area, the interior based estimation is unreliable and is significantly affected by noise as shown in figure 2. In contrast, the perimeter of the intrusion is more substantial than its area, and so the boundary-based estimation is able to estimate the shape's orientation more reliably despite the noise.

1.2 Determining Compound Shape Orientation

Computing shape orientation is a typical preprocessing task in image processing and computer vision applications. Consequently, use of inappropriate methods for determining object orientation would lead to a cumulative error at the end of the vision system's processing pipeline. Because of that, and because of the diversity of image processing and computer vision applications, the problem of reliably and accurately determining shape orientation is a perennial research topic, and many methods have already been developed; for recent examples see [32, 34]. Most of this work is done for single component shapes, whereas in this paper we introduce a method for computing the orientation of compound shapes. We consider a line that maximises the integral of the squared lengths of the projections of line segments whose end points belong the boundaries of particular shape components onto this line. Then we define the orientation of the shape by the slope of this line. It turns out that such a method for computing orientation of compound shapes, if applied to a single component shape, is consistent with the method that defines the shape's orientation by the line that minimises the integral of the squared distances of all boundary points to this line. It is worth mentioning that the latter method is analogous to the standard method which defines the shape orientation by the line that minimises the integral of squared distances of the points in the shape to the line. A use of a higher exponent than 2 (in the standard method) is studied in [31, 36]. Namely, it is well known that the standard method should be modified in order to be applicable to a wider class of shapes. A modification is introduced in [31] where the squared distances are replaced with distances to a higher power.

Here, we will not discuss a modification of the method that uses a higher exponent

$2N$ of the length projections (instead of squared ones) but such a modification is possible and relatively straightforward if the idea and approach from [37] is followed. It is worth mentioning that if such a modified method is applied to a single component shape then it is not consistent for $N > 1$ with the method which defines the shape's orientation by the line that minimises the integral of the distances, taken with the power of $2N$, of all boundary points to this line.

Notice that there is not a straightforward way to compute the orientation of a multi-component shape from the orientations (computed by some of the existing methods for single component shapes) of its components. Indeed, a very natural idea would be to compute the orientation of a compound shape from the orientations assigned to its components, probably weighted by some coefficients (e.g. a function of the component size). However, the problem is that almost all existing methods define the shape orientation by a line (not by a vector), implying that the computed orientations α and $\alpha + 180°$ are assumed to be the same. So, if S_1, S_2, ..., S_n are components of a multi-component shape S, then most of the existing methods would compute their orientations as $\varphi_1 + a_1 \cdot 180°$, $\varphi_2 + a_2 \cdot 180°$, ..., $\varphi_n + a_n \cdot 180°$, where the numbers a_1, a_2, ..., a_n are arbitrarily chosen from $\{0, 1\}$. Thus if, in the simplest variant, the orientation of $S = S_1 \cup S_2 \cup \ldots \cup S_n$ is computed as the average value of the orientations assigned to its components, then the orientation of S would be computed as

$$\frac{(\varphi_1 + a_1 \cdot 180°) + \ldots + (\varphi_n + a_n \cdot 180°)}{n} = \frac{\varphi_1 + \ldots + \varphi_n}{n} + \frac{(a_1 + \ldots + a_n) \cdot 180°}{n}$$

and obviously, for different choices of a_1, a_2, ..., a_n, the computed orientations are inconsistent (i.e. they could differ for an arbitrary multiple of the fraction $180°/n$). This is obviously unacceptable.

1.3 Anisotropy of Multiple Component Shapes

In the literature, shape orientation and shape elongation are very often considered together. The following scenario could be understood as a common approach: If orientation of a given shape S is defined by the direction for which the optimisation function $F(S, \alpha)$ reaches its maximum, then the elongation of S is defined as the ratio $\dfrac{\max_{\alpha \in [0,2\pi)} F(S, \alpha)}{\min_{\alpha \in [0,2\pi)} F(S, \alpha)}$.

Just as the concept of orientation can be extended from single component shapes to multiple components, elongation can also be applied to multiple components, and we will see that it effectively produces a measure of anisotropy. These two shape properties (orientation

and anisotropy) can be generally useful in computer vision, and have hundreds of applications in material science, medicine, engineering, geophysics, etc. To give just a few examples:

- Arnold [1] analysed the relationship between the orientation of fish larvae with respect to the direction of the current and various conditions (e.g. light intensity).
- Karátson *et al.* [15] quantified the strength of directional clast fabric (i.e. the anisotropy of rock fragments) in the flow of volcanic material so as to discriminate between types of deposits and provide evidence for emplacement mechanisms.
- Enomae *et al.* [6] measured the orientation angle and anisotropy of paper fibre since these values affect the physical properties of paper, such as its strength, shrinkage and curl. Moreover, they can also be used in the classification of ancient papers.
- Scharcanski and Dodson [27] also considered paper and other web-based materials such as polymer sheets, non-woven textiles, etc. A method for quantifying anisotropy was developed for application to on-line monitoring of continuous manufacturing processes.
- Saha and Wehrli [25] measured trabecular bone anisotropy since it has a significant effect on the bones biomechanical behaviour, and can therefore be used to check for disorders such as osteoporosis.
- The analysis of microstructure is important when designing new materials. Ganesh and Chawla [8] analysed the orientations of the reinforcement particles in metal matrix composites to check for a relationship between particle orientation and tensile strength.

1.4 Contents of This Paper

This paper makes several contributions. It extends our previous work on computing shape orientation based on the line maximising the integral of the squared lengths of the projections of line segments [37]. Whereas that previous work operated on the shape interior (the endpoints of the line segments were defined to lie inside the shape) the current work adapts this approach to provide a different, boundary-based orientation instead. The method is further extended in this paper to develop a new measure of anisotropy.

The paper is organised as follows. A short overview of the standard method for computation of shape orientation is given in section 2.

Section 3 introduces the new method for computing orientation of multi component shapes, explains the basic idea and motivation. Also, the same section gives several modification of the new method. Those methods enable a control of the impact of the components size to the computed orientation of the compound shape. In section 3 we extend the method to compound shapes and make some notes regarding its properties. In section 4 the idea of the standard region-based measure of elongation is adapted to a boundary-based measure over multiple components, effectively providing a measure of anisotropy. Section 5 demonstrates the results of computing orientation and anisotropy on several different data sets. Finally, concluding comments are given in section 6.

2 The Standard Method for Single Component Shapes

Before considering the definition of orientation of compound shapes, what will be done in the next section, we give a short overview of the most standard methods for the computation of orientation of a single component shape. The most standard area based method, for the computations uses the geometric (area) moments is based on a use the axis of the least second moment of inertia [31, 36]. More precisely, the axis of the least second moment of inertia [14, 16] is the line which minimises the integral of the squares of distances of the points (belonging to the shape) to the line. The integral is

$$I(\alpha, S, \rho) = \iint_S r^2(x, y, \alpha, \rho)\ dx\ dy \tag{1}$$

where $r(x, y, \alpha, \rho)$ is the perpendicular distance from the point (x, y) to the line given in the form $X \cdot \sin\alpha - Y \cdot \cos\alpha = \rho$. The angle which minimizes the above integral can be easily computed [31], and is used to define the orientation of the shape S. So, the following formal definition is natural.

Definition 1 *The orientation of a given shape S is given by the angle α for which the function $I(\alpha, S, \rho)$ reaches the minimum.*

If someone would like to use the boundary points only, to define the shape orientation, then the line moments $\mu_{p,q}(\partial S)$ along the contour ∂S, (i.e. the boundary of a given shape S), should be used instead of the geometric (area) moments and a similar reasoning can be

applied [3]. More formally, for the contour ∂S representing the boundary of S and given in its arc length parametrisation $x = x(s)$, $y = y(s)$, $s \in [0, per(S)]$, the line moment $\mu_{p,q}(\partial S)$, is defined by

$$\mu_{p,q}(\partial S) = \int_{\partial S} x(s)^p \; y(s)^q \; ds, \tag{2}$$

while the centralised line moments $\overline{\mu}_{p,q}(\partial S)$ is defined as

$$\overline{\mu}_{p,q}(\partial S) = \int_{\partial S} \left(x(s) - \frac{\mu_{1,0}(\partial S)}{\mu_{0,0}(\partial S)} \right)^p \; \left(y(s) - \frac{\mu_{0,1}(\partial S)}{\mu_{0,0}(\partial S)} \right)^q \; ds. \tag{3}$$

Now, the orientation of S, based only on the information from its boundary ∂S, is defined by the angle α that minimises the function

$$E(\alpha, \partial S) = \int_{\partial S} \left(\left(x - \frac{\mu_{1,0}(\partial S)}{\mu_{0,0}(\partial S)} \right) \cdot \sin\alpha - \left(y - \frac{\mu_{0,1}(\partial S)}{\mu_{0,0}(\partial S)} \right) \cdot \cos\alpha \right)^2 \; ds \tag{4}$$

i.e.

$$\begin{aligned} E(\alpha, \partial S) \;\; &= \;\; \left(\mu_{2,0}(\partial S) - \frac{(\mu_{1,0}(\partial S))^2}{\mu_{0,0}(\partial S)} \right) \cdot \sin^2\alpha + \left(\mu_{0,2}(\partial S) - \frac{(\mu_{0,1}(\partial S))^2}{\mu_{0,0}(\partial S)} \right) \cdot \cos^2\alpha \\ &- \;\; \left(\mu_{1,1}(\partial S) - \frac{\mu_{1,0}(\partial S) \cdot \mu_{0,1}(\partial S)}{\mu_{0,0}(\partial S)} \right) \cdot \sin(2\alpha). \end{aligned} \tag{5}$$

Notice that $E(\alpha, \partial S)$ equals the integral of the squared distances of all the boundary points of S to the line that passes the point $\left(\frac{\mu_{1,0}(\partial S)}{\mu_{0,0}(\partial S)}, \frac{\mu_{0,1}(\partial S)}{\mu_{0,0}(\partial S)} \right)$ and has the slope α. Such a line is described by the equation $\left(X - \frac{\mu_{1,0}(\partial S)}{\mu_{0,0}(\partial S)} \right) \cdot \sin\alpha - \left(Y - \frac{\mu_{0,1}(\partial S)}{\mu_{0,0}(\partial S)} \right) \cdot \cos\alpha = 0$. Thus, the following definition for boundary-based shape orientation is an analogue for the standard method for the computing shape orientation.

Definition 2 *Let S be a given shape. The orientation of S is defined by the angle α where the function $E(\alpha, \partial S)$ reaches its minimum.*

It is easy to verify that such an angle α satisfies the following equation

$$\tan(2\alpha) = \frac{2\overline{\mu}_{1,1}(\partial S)}{(\overline{\mu}_{2,0}(\partial S))^2 - (\overline{\mu}_{0,2}(\partial S))^2}. \tag{6}$$

3 Orientation of Compound Shapes

In this section we use idea of [37] and introduce a method for computing the boundary based orientation of compound shapes. Informally speaking, we consider all the line segments whose end points belong to a particular shape component and define the orientation of the compound shape by the line which maximises squared projections of such line segments onto this line. Thus, it can be said that such a defined orientation is based on the orientations of the shape components rather than determining orientation as a global property of the compound shape. We continue with a more formal definition.

Let S be a compound object consisting of m components S_1, S_2, ..., S_m whose boundaries ∂S_1, ∂S_2, ..., ∂S_m are given in an arc length parametric form $x_i = x_i(s)$, $y_i = y_i(s)$, $s \in [0, per(S_i)]$, where $per(S_i) = \int_{\partial S_i} ds$ is the length of the contour ∂S_i. For each component S_i, let consider all the line segments $[A_iB_i]$ whose end points A_i and B_i belong to the boundary ∂S_i. In other words,

$$A_i = A_i(s) = (x_i(s), y_i(s)) \quad \text{and} \quad B_i = B_i(l) = (x_i(l), y_i(l)) \qquad \text{for some} \quad s, l \in [0, per(S_i)].$$

Further, let

- $\overrightarrow{a}$ denote the unit vector in the direction α, i.e. $\overrightarrow{a} = (\cos\alpha, \sin\alpha)$,
- $\mathbf{pr}_{\overrightarrow{a}}[AB]$ be the projection of the line segment $[AB]$ onto a line that makes an angle α with the x-axis, and
- $|\mathbf{pr}_{\overrightarrow{a}}[AB]|$ denotes the length of such a projection.

Now, we give the following definition for orientation of compound shapes.

Definition 3 *Let S be a compound object consisting of m components S_1, S_2, ..., S_m, and let ∂S denotes the boundary of S, i.e. $\partial S = \cup_{i=1}^{m} \partial S_i$ is the union of boundaries ∂S_i of components S_i of S. Then the orientation of S is defined by the angle that maximises the function $L_{comp}(\alpha, \partial S)$ defined by*

$$L_{comp}(\alpha, \partial S) = \sum_{i=1}^{m} \int\int_{\substack{s\in[0,per(S_i)] \\ l\in[0,per(S_i)]}} |\mathbf{pr}_{\overrightarrow{a}}[A_i(s)B_i(l)]|^2 ds\ dl. \tag{7}$$

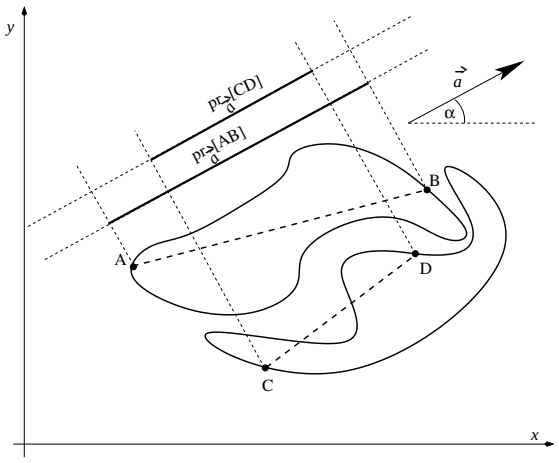

Figure 3: Projections of all the line segments whose endpoints lie on the boundary of a particular component S_i of the given compound shape S are considered, irrespective of whether the line segment intersects the boundary ∂S_i (e.g. the line segment $[CD]$) or not (e.g. $[AB]$).

Definition 3 can be understood as a natural one, taking into account that we are looking for a definition of the orientation of compound shapes which takes into account the boundary information only. Once again, Definition 3 considers all the edges whose end points belong to the boundary of certain component of S, and then defines the orientation S by the line that maximises the sum of the squared projections of such edges onto this line.

A very desirable property of such a defined orientation is that it enables easy computation. That is the result of the following theorem. To prove the statement, only elementary mathematics is needed. The proof is omitted, since the same formalism could be applied as in the proof of Theorem 2 from [37].

Theorem 1 *The angle α where the function $L_{comp}(\alpha, \partial S)$ reaches its maximum satisfies the following equation*

$$\tan(2\alpha) = \frac{2 \cdot \sum_{i=1}^{m} (\mu_{1,1}(\partial S_i) \cdot \mu_{0,0}(\partial S_i) - \mu_{1,0}(\partial S_i) \cdot \mu_{0,1}(\partial S_i))}{\sum_{i=1}^{m} ((\mu_{2,0}(\partial S_i) - \mu_{0,2}(\partial S_i)) \cdot \mu_{0,0}(\partial S_i) + (\mu_{0,1}(\partial S_i))^2 - (\mu_{1,0}(\partial S_i))^2)}$$

$$= \frac{2 \cdot \sum_{i=1}^{m} \overline{\mu}_{1,1}(\partial S_i) \cdot \mu_{0,0}(\partial S_i)}{\sum_{i=1}^{m} (\overline{\mu}_{2,0}(\partial S_i) - \overline{\mu}_{0,2}(\partial S_i)) \cdot \mu_{0,0}(\partial S_i)}. \tag{8}$$

We proceed with the lemma which shows that the standard, boundary based method, for computing the shape orientation orientation (see Definition 2) is a particular case of the method for computing the orientation of compound shapes introduced in this paper. If we specify that the shape S from Definition 3 is a single component shape then such a restriction leads to the following definition for the orientation of a single component shape S.

Definition 4 *For a given shape S the orientation of S is defined by the angle α where the function*

$$L(\alpha, \partial S) = \int\int_{\substack{s \in [0, per(S)] \\ l \in [0, per(S)]}} |\mathbf{pr}_{\overrightarrow{a}}[A(s)B(l)]|^2 \; ds \; dl \tag{9}$$

reaches its maximum.

Even though Definition 2 and Definition 4 come from different motivations it turns out that they are equivalent. We give the following lemma.

Theorem 2 *Let S be a single component shape, then the orientation of S computed by Definition 4 is the same as the orientation computed by Definition 2.*

Proof. By using definitions of $L(\alpha, \partial S)$ and $E(\alpha, \partial S)$ (see (9) and (5)) we easily derive:

$$\begin{aligned} & L(\alpha, \partial S) + 2 \cdot \mu_{0,0}(\partial S) \cdot E(\alpha, \partial S) \\ = \; & 2 \cdot (\mu_{2,0}(\partial S) + \mu_{0,2}(\partial S)) \cdot \mu_{0,0}(\partial S) - 2 \cdot (\mu_{1,0}(\partial S))^2 - 2 \cdot (\mu_{0,1}(\partial S))^2. \end{aligned} \tag{10}$$

A direct consequence of the previous equality is that the quantity

$$L(\alpha, \partial S) + 2 \cdot \mu_{0,0}(\partial S) \cdot E(\alpha, \partial S) \tag{11}$$

depends only on the shape S but not on the angle α.

Further, this implies that the maximum of $L(\alpha, \partial S)$ and minimum of $E(\alpha, \partial S)$ must be reached at the same point. In other words, the orientations computed by Definition 2 and Definition 4 are consistent, which establishes the proof. □

Note. *Notice that specifying $m = 1$ in the equation (8), in Theorem 1, we obtain that the orientation α of a single component shape S computed by the new method satisfies the equation*

$$\tan(2\alpha) = \frac{2 \cdot \overline{\mu}_{1,1}(\partial S) \cdot \mu_{0,0}(\partial S)}{(\overline{\mu}_{2,0}(\partial S) - \overline{\mu}_{0,2}(\partial S)) \cdot \mu_{0,0}(\partial S)}.$$

The same equation is satisfied by the orientation angle β computed by the standard method (see Definition 2 and the equation (6) thereafter). Thus,

$$\tan(2\alpha) = \tan(2\beta)$$

holds. But Theorem 2 gives more:

- *The orientations α and β computed by the standard method and the new one, respectively, satisfy the equality $\tan(2\alpha) = \tan(2\beta)$ but Theorem 2 excludes the possibility $\alpha = \beta + \frac{\pi}{2}$. I.e. Theorem 2 says that it must be $\alpha = \beta$.*
- *The derived equation (10) fully describes the relationship between the optimising functions $E(\alpha, \partial S)$ and $L(\alpha, \partial S)$ used in the standard method and the method developed here.*

Being naturally defined and theoretically well founded, the behaviour of the new method for computing the compound shapes orientation can be well understood. Also, in some particular situations such a behaviour can be predicted very precisely. We illustrate this by the following lemma which summarises how the new method behaves in some canonical situations, including the situations when the method brakes down.

Lemma 1 *The new method for the computation of the orientation of compound shapes has the following properties.*

(a) Let a compound shape $S = S_1 \cup \ldots \cup S_m$. The new method breaks down when

$$\sum_{i=1}^{m} \overline{\mu}_{1,1}(\partial S_i) \cdot \mu_{0,0}(\partial S_i) = \sum_{i=1}^{m} \left(\overline{\mu}_{2,0}(\partial S_i) - \overline{\mu}_{0,2}(\partial S_i)\right) \cdot \mu_{0,0}(\partial S_i) = 0 \qquad (12)$$

(i.e. the optimizing function $L_{comp}(\alpha, \partial S)$ is then constant).

(b) Let a compound shape $S = S_1 \cup \ldots \cup S_m$ and let $L(\alpha, \partial S_i) = constant$ for $i = 1, \ldots, k$ where $k < m$. Then

$$L_{comp}(\alpha, \partial S_1 \cup \ldots \cup \partial S_k \cup \partial S_{k+1} \cup \partial S_m) = L_{comp}(\alpha, \partial S_{k+1} \cup \ldots \cup \partial S_m).$$

(I.e., the new method gives the same orientation for the compound shapes $S_1 \cup \ldots \cup S_m$ and $S_{k+1} \cup \ldots \cup S_m$. So, the components $S_1, \ldots, S_k$ can be ignored when computing the orientation of $S_1 \cup \ldots \cup S_m$).

(c) If all components of S have identical orientation according to $L(\alpha, \partial S)$ then this same orientation is also computed by $L_{comp}(\alpha, \partial S)$).

Proof. Since the proof is similar to the proof of the analogous statements for the area based measure from [37], it is omitted. □

The differences between the standard and new methods for computing orientation are demonstrated clearly in figure 4(a). The data consists of several components (coloured black or gray), which are split into two sets according to the overlaid central dividing line. Orientation is computed both separately for the left and right sets of components, and is also computed for the combined set. As expected, the results for the standard method depend on the distribution of the components, and so the orientations for the three sets vary substantially. In contrast, the new method produces very consistent orientations for the three sets. A similar effect occurs in figure 4(b), where an image of embryonic tissue is split onto two parts. Again, the new method produces very consistent orientations for the upper part (coloured gray), lower part (coloured black) and the whole image, whereas the standard method produces inconsistent orientations.

3.1 Components Size Dependent Method

As in the case of the area based method for the computation of the orientation of multi-component shapes [37], the new (boundary based) method allows modifications which enable to control the impact of the perimeter of the shape components to the computed shape orientation. Moreover, there is also a modification which does not take into account the component perimeters at all, which could be desirable in some applications. Note that the size of shape components, as measured in a given image, are dependent on the position of the original object components with respect to the camera. Thus, such a modified method would be able to correct such a (very often) unacceptable influence of the relative components position with respect to the camera.

As in [37], can use a simple two-component shape to illustrate our conclusions. So, if we consider a two-component shape $S = S_1 \cup S_2'$ where S_2' is the dilation of a shape S_2 by a

(a): 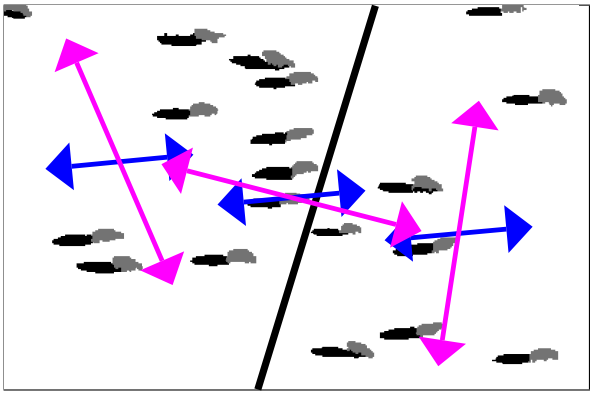 **(b):** 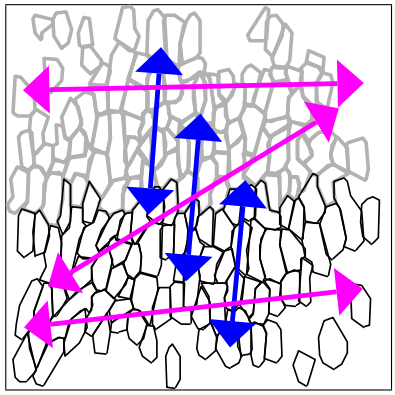

Figure 4: **(a):** The components are coloured black or gray, and are separated into sets by the central dividing line. Orientations computed for the left, right and combined sets are shown overlaid for the standard method (long arrows) and the new method (short arrows). **(b):** Similarly, an embryonic tissue image is split onto two parts. Orientations computed for the lower part, upper part and whole image are shown overlaid for the standard method (long arrows) and the new method (short arrows).

factor $\mathbf{r}$, i.e. $S_2' = \mathbf{r} \cdot S_2 = \{(\mathbf{r} \cdot x, \mathbf{r} \cdot y) \mid (x, y) \in S_2\}$, then the orientation α of S, computed by (8), is computed from

$$\tan(2\alpha) = \frac{2 \cdot \overline{\mu}_{1,1}(\partial S_1) \cdot \mu_{0,0}(\partial S_1) + 2 \cdot \mathbf{r}^4 \cdot \overline{\mu}_{1,1}(\partial S_2) \cdot \mu_{0,0}(\partial S_2)}{(\overline{\mu}_{2,0}(\partial S_1) - \overline{\mu}_{0,2}(\partial S_1)) \cdot \mu_{0,0}(\partial S_1) + \mathbf{r}^4 \cdot (\overline{\mu}_{2,0}(\partial S_2) - \overline{\mu}_{0,2}(\partial S_2)) \cdot \mu_{0,0}(\partial S_2)}.$$

Obviously, the influence of S_2' to the computed orientation of S is proportional to $\mathbf{r}^4$ and could be very big if the dilation factor $\mathbf{r}$ is much bigger than 1. To reduce such a large effect we can apply the following formula:

$$\tan(2\alpha) = \frac{2 \cdot \sum_{i=1}^{m} \overline{\mu}_{1,1}(\partial S_i)/(m_{0,0}(\partial S_i))^2}{\sum_{i=1}^{m} (\overline{\mu}_{2,0}(\partial S_i) - \overline{\mu}_{0,2}(\partial S_i))/(m_{0,0}(\partial S_i))^2}, \tag{13}$$

which enforce instead a linear weighting by perimeter (i.e. an influence proportional to $\mathbf{r}$).

Whilst a linear weighting by perimeter (given by (13)) seems reasonable in most circumstances, another possibility that may be suitable for some applications is that the weight of a component is completely independent of its size (for example, see the gait analysis example

in [37]). This can be enforced using the following formula:

$$\tan(2\alpha) = \frac{2 \cdot \sum_{i=1}^{m} \overline{\mu}_{1,1}(\partial S_i)/(m_{0,0}(\partial S_i))^3}{\sum_{i=1}^{m} (\overline{\mu}_{2,0}(\partial S_i) - \overline{\mu}_{0,2}(\partial S_i))/(m_{0,0}(\partial S_i))^3}. \tag{14}$$

In the view of the previous simple example, if the last formula is applied then the computed orientation α satisfies:

$$\tan(2\alpha) = \frac{2 \cdot \overline{\mu}_{1,1}(\partial S_1)/(\mu_{0,0}(\partial S_1))^3 + 2 \cdot \overline{\mu}_{1,1}(\partial S_2)/(\mu_{0,0}(\partial S_2))^3}{(\overline{\mu}_{2,0}(\partial S_1) - \overline{\mu}_{0,2}(\partial S_1))/(\mu_{0,0}(\partial S_1))^3 + (\overline{\mu}_{2,0}(\partial S_2) - \overline{\mu}_{0,2}(\partial S_2))/(\mu_{0,0}(\partial S_2))^3} \tag{15}$$

and obviously, the computed orientation (i.e. $\tan(2\alpha)$) does not depend on $\mathbf{r}$. It is easy to verify that the same holds if a given shape consists of more than two components.

4 Anisotropy Measure

As mentioned in the introduction, a shape's orientation and elongation are often considered together. If the orientation of a given shape S is defined by the direction for which an optimising function $F(S, \alpha)$ reaches its extreme value, then a common approach is to define the elongation of S as the ratio $\frac{\max_{\alpha \in [0,2\pi)} F(S,\alpha)}{\min_{\alpha \in [0,2\pi)} F(S,\alpha)}$. But it turns out that in the case of multiple component shapes, the meaning of such a ratio describes the anisotropy of a set of multiple components rather than its elongation (in the sense of the ordinary meaning of these words).

To be exact, in the case of compound shapes $S_1 \cup \ldots \cup S_m$, we will consider the ratio

$$\frac{\max_{\alpha \in [0,2\pi)} L_{comp}(\alpha, \partial S)}{\min_{\alpha \in [0,2\pi)} L_{comp}(\alpha, \partial S)}$$

and will call it a *compound shape anisotropy measure* since it is maximised when all components are aligned in the same direction, as shown by the following theorem.

Theorem 3 *Let S be a compound shape whose components are S_1, S_2, ..., S_m, and each of the components of S_i has orientation α_i where α_i is computed by maximising $L(\alpha, \partial S_i)$. Then the ratio $\frac{\max_{\alpha \in [0,2\pi)} L_{comp}(\alpha, \partial S)}{\min_{\alpha \in [0,2\pi)} L_{comp}(\alpha, \partial S)}$ reaches its maximum if $\alpha_i = \alpha_2 = \ldots = \alpha_m$.*

Proof. We start from Definitions 3 and 4 and show that the nominator and denominator reach their maximum and minimum value (respectively) if and only if the components of S have the same orientation, i.e. if and only if $\alpha_i = \alpha_2 = \ldots = \alpha_m$. So,

$$\max_{\alpha\in[0,2\pi]}\{L_{comp}(\alpha,\partial S)\} = \max_{\alpha\in[0,2\pi]}\left\{\sum_{i=1}^{m} L(\alpha,\partial S_i)\right\} \leq \sum_{i=1}^{m}\max_{\alpha\in[0,2\pi]}\{L(\alpha,\partial S_i)\} = \sum_{i=1}^{m} L(\alpha_i,\partial S_i). \tag{16}$$

Thus, an upper bound for $\max_{\alpha\in[0,2\pi]}\{L_{comp}(\alpha,\partial S)\}$ is $\sum_{i=1}^{m} L(\alpha_i,\partial S_i)$ and this upper bound is obviously reached if $\alpha_i = \alpha_2 = \ldots = \alpha_m$, i.e. then $\max_{\alpha\in[0,2\pi]}\{L_{comp}(\alpha,\partial S)\} = \sum_{i=1}^{m} L(\alpha_i,\partial S_i)$.

On the other hand, if for two components, say S_p and S_q, the functions $L(\alpha,\partial S_p)$ and $L(\alpha,\partial S_q)$ reach their maxima for a different angle, then $\max_{\alpha\in[0,2\pi]}\{L(\alpha,\partial S_p)+L(\alpha,\partial S_q)\} < \max_{\alpha\in[0,2\pi]}\{L(\alpha,\partial S_p)\} + \max_{\alpha\in[0,2\pi]}\{L(\alpha,\partial S_q)\}$ which further implies that the inequality in (16) is also strict.

This completes the proof that the greatest possible value of $\max_{\alpha\in[0,2\pi]}\{L_{comp}(\alpha,\partial S)\}$ is reached if and only if all the component S_i of S have the same orientation.

To prove that the smallest possible value of $\min_{\alpha\in[0,2\pi]}\{L_{comp}(\alpha,\partial S)\}$ is reached if and only if all the components of S have the same orientation, we should start from

$$\min_{\alpha\in[0,2\pi]}\{L_{comp}(\alpha,\partial S)\} = \min_{\alpha\in[0,2\pi]}\left\{\sum_{i=1}^{m} L(\alpha,\partial S_i)\right\} \geq \sum_{i=1}^{m}\min_{\alpha\in[0,2\pi]}\{L(\alpha,\partial S_i)\}. \tag{17}$$

and apply similar reasoning as for (16). □

Based on Theorem 3 it seems natural to define the anisotropy shape measure by using the ratio $\dfrac{\max_{\alpha\in[0,2\pi)} L_{comp}(\alpha,\partial S)}{\min_{\alpha\in[0,2\pi)} L_{comp}(\alpha,\partial S)}$. We give the following formal definition.

Definition 5 *Let S be a compound shape whose components are S_1, S_2, ..., S_m. Then the anisotropy $\mathcal{A}(S) = \mathcal{A}(S_1 \cup S_2 \cup \ldots \cup S_m)$ of S is defined as*

$$\mathcal{A}(S) \;=\; \frac{\max_{\alpha\in[0,2\pi)} L_{comp}(\alpha,\partial S)}{\min_{\alpha\in[0,2\pi)} L_{comp}(\alpha,\partial S)}. \tag{18}$$

The compound shape anisotropy measure $\mathcal{A}(S)$, defined as above, indicates how consistent the orientations of the components comprising a shape are. It has the following properties:

- $\mathcal{A}(S)$ ranges over $[1,\infty)$;

- $\mathcal{A}(S)$ is translation, rotational and scaling invariant;
- $\mathcal{A}(S)$ is also easy to compute (as shown by the next theorem).

The following theorem (for a proof see Appendix A) gives a closed formula for the computation of $\mathcal{A}(S)$.

Theorem 4 *Let S be a compound shape whose components are S_1, S_2, ..., S_m. Then*

$$\mathcal{A}(S) = \mathcal{A}(S_1 \cup S_2 \cup \ldots \cup S_m) = \frac{C + \sqrt{A^2 + B^2}}{C - \sqrt{A^2 + B^2}} \tag{19}$$

where

$C = \sum_{i=1}^{m} (\overline{\mu}_{2,0}(\partial S_i) + \overline{\mu}_{0,2}(\partial S_i))\mu_{0,0}(\partial S_i)$, $\quad A = \sum_{i=1}^{m} (\overline{\mu}_{2,0}(\partial S_i) - \overline{\mu}_{0,2}(\partial S_i))\mu_{0,0}(\partial S_i)$ *and*

$B = \sum_{i=1}^{m} 2\overline{\mu}_{1,1}(\partial S_i)\mu_{0,0}(\partial S_i)$.

Roughly speaking, the anisotropy measure, as given by Definition 5, primarily depends on the consistency of the orientations of the shape's components, but also on the elongation of the components. E.g. consider two compound shapes such that the components in each shape are mutually the same and have the same orientation. A higher anisotropy value will be assigned to the shape whose components are more elongated (formally to the shape whose components have the larger ratio $\frac{\max_{\alpha\in[0,2\pi]}\{L(\alpha,S_i)\}}{\min_{\alpha\in[0,2\pi}\{L(\alpha,S_i)\}}$). This is a desirable property. Notice that the effects of a component's elongation could be controlled (if necessary) by some modifications of the definition. In addition, for shapes which do not consist of identical components, the influence of a component's size could also be controlled by modifications similar to those in subsection 3.1.

We give a few examples to demonstrate the anisotropy measure. Each image in figure 5 is treated as a multiple component object (e.g. a herd of cattle). For the image in figure 5a the anisotropy was first computed for just the cattle, giving a value of 3.49, which is appropriate since they are mostly facing in the same direction. The anisotropy of the cattle's shadows alone increases to 7.57 since the shadows are more consistently orientated, and are also slightly more elongated. Merging the cattle and their shadows produces even more elongated regions, and so the herd's anisotropy further increases to 12.08. Another example of somewhat elongated shapes which are approximately aligned in one direction is given by the yachts moored in figure 5b, and again the anisotropy value of 4.65 is much greater than 1.

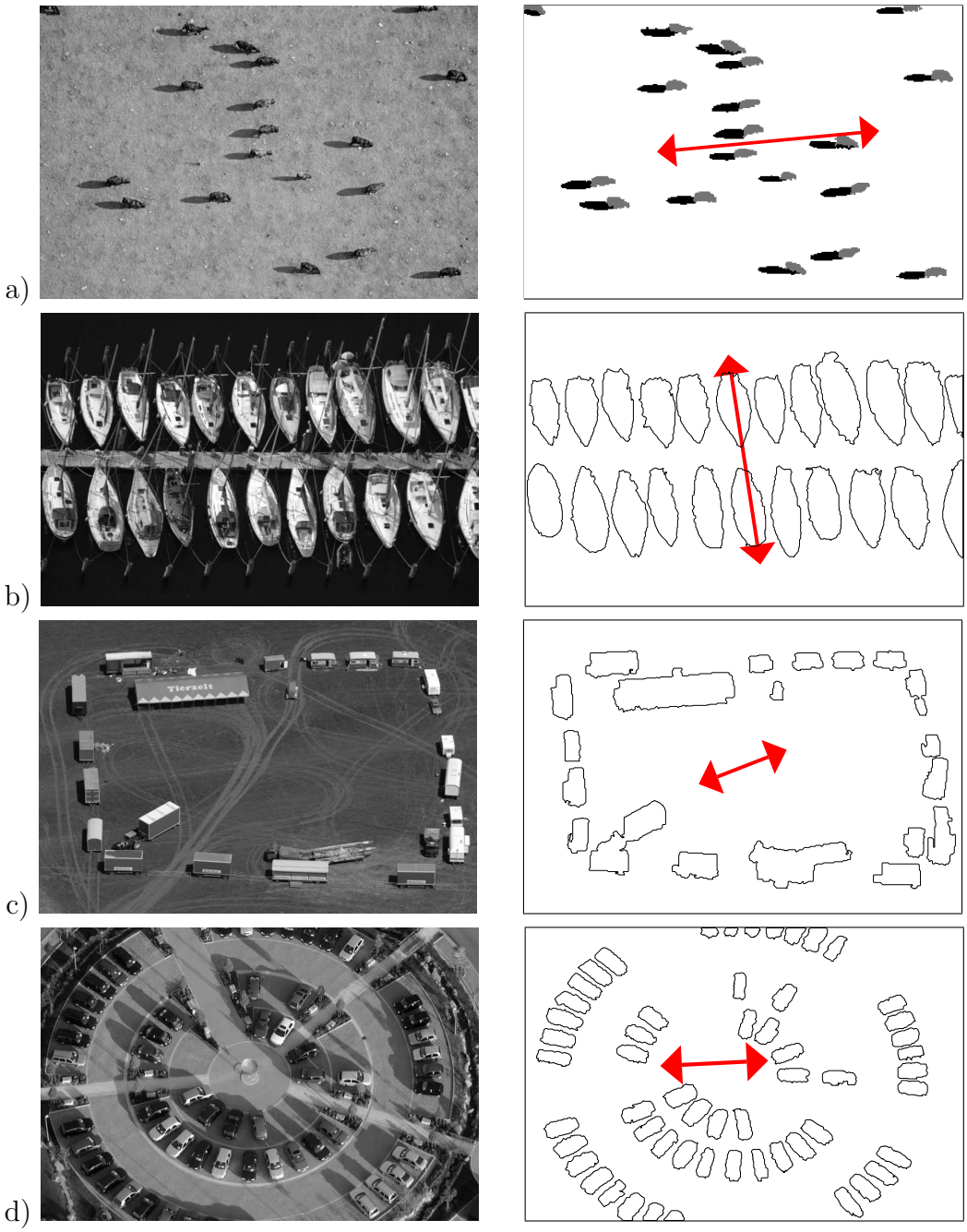

Figure 5: Images and extracted object boundaries. For each image the set of boundaries is treated as a multiple component object. The computed orientations are displayed as arrows with length proportional to $1 - \frac{1}{\mathcal{A}(S)}$.

In comparison, the remaining examples contain components distributed over two (figure 5c) or more (figure 5d) orientations which causes the anisotropy values to be much lower (1.33, 1.38 respectively) even though the individual components are elongated.

5 Examples

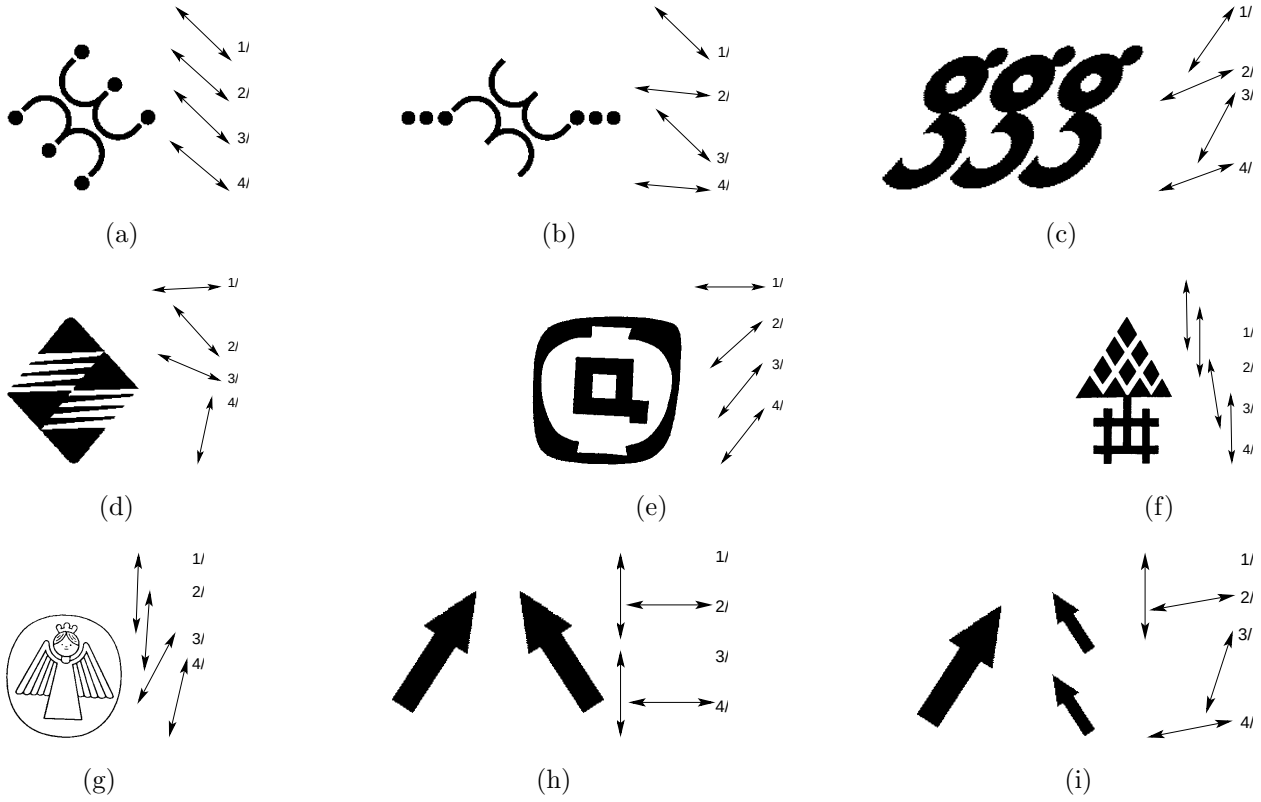

Figure 6: Orientations are displayed as arrows in the order: 1/ boundary method treating shape as multiple components, 2/ boundary method treating shape as single object, 3/ interior method treating shape as multiple components, 4/ interior method treating shape as single object.

The following provides some examples of applying the proposed methods. Where the input data consists of (binarized) images, the boundaries have been extracted. Rather than calculating the moments from the boundary pixels, polygonal approximations of the boundaries are generated using Ramer's algorithm [24] with a threshold of two unless specified otherwise. The line moments are then directly calculated from the polygon or polyline [18].

In figure 6 we present results of computing the orientation of trademarks which consist of multiple components. The results are compared when orientations are obtained by i) treating the shapes as single entities versus multiple components, and ii) analysis of shape boundary versus shape interior. First, it is possible for all these four combinations of approaches to coincide, as in the example in figure 6a which contains two curvilinear structures and six balls. For the component based approaches the curvilinear structures dominate the orientation estimation since not only are they larger than the balls, but are elongated and therefore much more orientable. In fact, the balls have negligible effect on the component based orientation values, which is desirable since their computed individual orientations are dependent on just digitisation and noise effects. Consequently, if the balls are moved outwards (figure 6b) then the component based orientations are unaltered, although the balls now dominate the globally measured orientation since they lie far from the global centroid.

Figure 6c shows an instance of a repeated shape, and (unlike the global orientation) both methods which explicitly deal with multiple components identify the overall orientation to be the same as the individual component orientations.

The trademark in figure 6d is made up of two parts, an upper and lower half. In terms of interior mass each component has a diagonal trend, whereas the multiple narrow indentations create a large portion of boundary along the horizontal. This results in differences in the boundary-based and interior-based method multiple component methods as they produce orientations aligned as above.

The difference in the boundary-based multiple component orientation for the shape in figure 6e compared to the interior-based multiple component orientation is due to several factors. First, the corners of the outer ring of the shape are thicker on one of the diagonals compared to the other, and this extra area is sufficient to fix the orientation chosen by the interior-based method. Second, the two rings produce four nested boundaries, but not all of these affect the computation of the interior-based method. In fact, counting outwards from the centre, the first and third boundaries are sufficiently symmetrical that they are essentially unorientable using the moments based approach. This is confirmed by their values of $\overline{\mu}_{1,1}(S_i)/(\mu_{0,0}(S_i))^2$ and $(\overline{\mu}_{2,0}(S_i)-\overline{\mu}_{0,2}(S_i))/(\mu_{0,0}(S_i))^2$ which are $\{0.01, 0.03\}$, $\{1.09, 1.00\}$, $\{-0.19, -0.38\}$, $\{-0.89, 0.10\}$. That is, the first and third pairs of values are close to zero. Thus, the second boundary (the Q-shape) is the most orientable component of the shape, and this dominates the final computed orientation.

The shape in figure 6f is essentially symmetric, and the orientations are closely aligned with the axis of symmetry since the shape is reasonably elongated. However, there is some distortion, most evident in the leftmost triangle which is part of the largest component. This affects the interior-based multiple component method most. Since the perimeter of that component is less affected distortion the boundary-based multiple component estimation of orientation is less affected, and is closer to the axis of symmetry.

Figure 6g shows a marked difference between the interior and boundary-based methods. In terms of size, there are two main components, the outer ring, and almost the complete angel with the exception of the hair and facial details. The angel shape is nearly vertical according to the interior-based method, but the outer ring is determined to be horizontal, and the combined effects of these two components produces an orientation in between, but more influenced by the larger angel shape. In contrast, the thin lines making up the angel mean that it has a substantially larger perimeter than the outer ring, and therefore the boundary-based multiple component estimation of orientation is overwhelmingly dominated by its vertical orientation.

Because the two arrows in figure 6h have a fairly wide horizontal separation the global methods compute a horizontal orientation. The arrows themselves are more consistent with a vertical orientation, as computed by both the multiple component methods. When the right-hand arrow is scaled in X and Y by a factor of 0.5 and duplicated (see figure 6i) then the alteration causes the global methods to produce new orientations. If the boundary-based multiple component method is applied with a linear weighting by perimeter then, as expected, the change has no effect. The interior-based multiple component was also applied with linear weighting by area, which naturally results in an alteration in orientation. Of course, the interior-based multiple component method can also be modified to use alternative area based weightings [37].

The second example applies multiple component orientation estimation and anisotropy to perform orientation normalisation (as shown in figure 7) in which it is applied as a step towards deskewing scanned pages of text. The images are thresholded and polygonal approximations to the extracted boundaries are formed using Ramer's algorithm [24] with a small threshold (i.e. a maximum deviation of one) since the letters are relatively small (20-70 pixels high). Although the characters are not generally vertically aligned, the idea is that if the pages contain sufficient characters then the distribution of characters within each

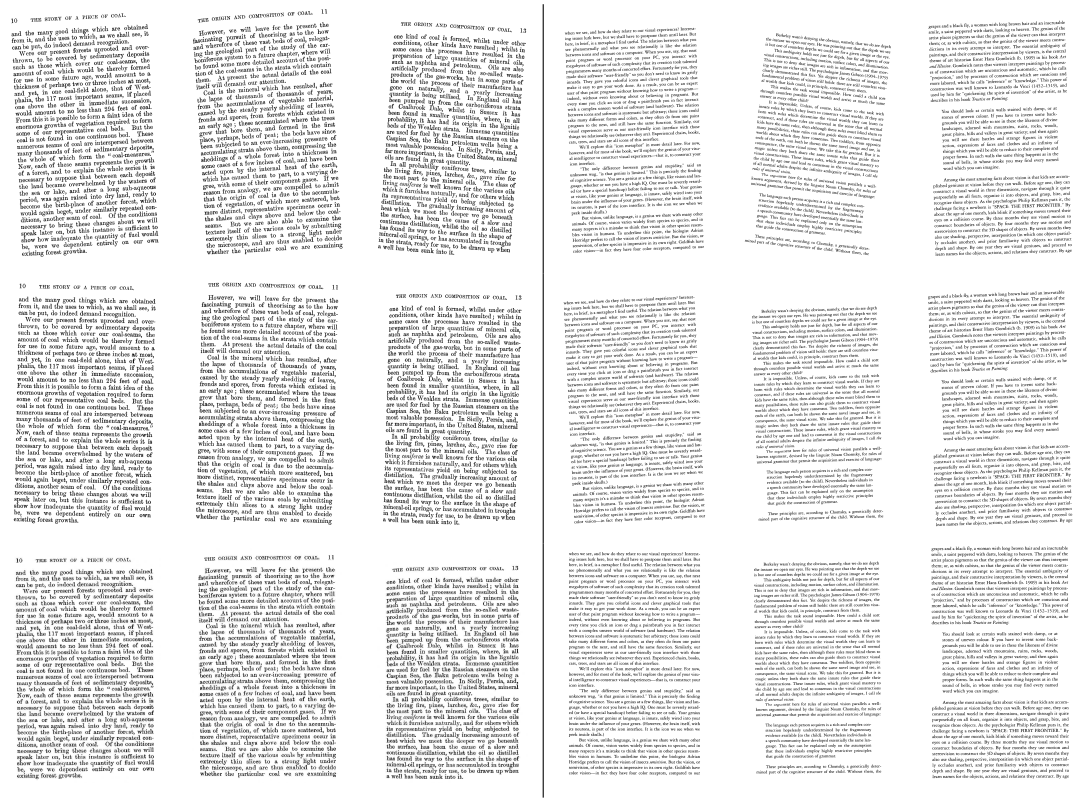

Figure 7: Thresholded pages from two books as scanned (first row) and after character based orientation normalisation (second row), and line based orientation normalisation (third row)

page should be similar, and so the orientations computed from each page's set of characters should be fairly consistent over a book. Experiments show that the results shown in figure 7 are typical and that the estimated orientations of a book's pages lie within an interval of 1°. To complete the deskewing process the pages would have to be further rotated by a constant amount determined from knowledge of the font or else from a sample page. Since this method operates on just the individual characters irrespective of their placement it is applicable even for very irregularly spaced text.

We can also use the compound component anisotropy measure to tackle the page deskewing problem in a different manner. Unlike our previous approach we now assume a traditional page layout with characters and words forming well defined straight lines. The idea is to blur the image so that the characters merge into maximally consistently elongated lines – i.e. maximally anisotropic. The set of lines extracted after thresholding makes up the compound shape from which the orientation can be computed. Since by definition the components are

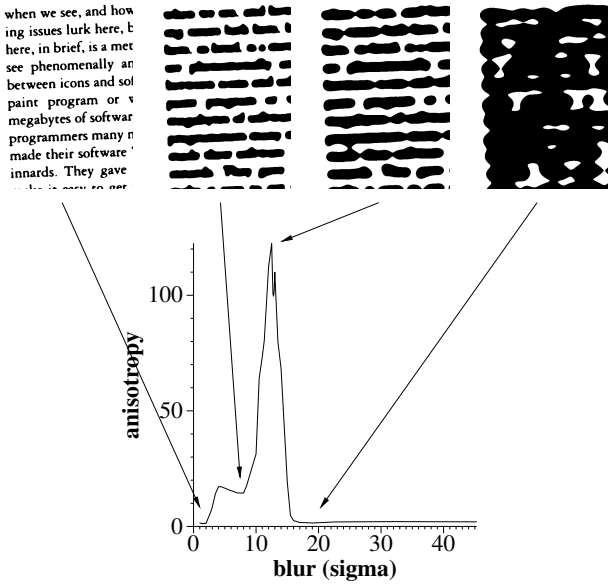

Figure 8: One of the page images from figure 7 is blurred and thresholded, and the resulting component anisotropy is plotted. A small portion of some of the thresholded images is shown demonstrating that maximum anisotropy is achieved when many of the words are merged into lines.

elongated, so their orientation should be distinct.

The process is demonstrated in figure 8. The graph shows that with little smoothing the components – which are initially mainly individual characters – are not consistently elongated. Further smoothing merges characters into words which now exhibit a reasonably pronounced anisotropy. However, it is when enough blurring is applied to merge characters into continuous lines that the anisotropy increases dramatically. More blurring is counter productive as sections of adjacent lines merge, and their anisotropy quickly drops. The results of deskewing using the estimated blur values are shown in the bottom row of figure 7, and it can be see that the pages are all correctly re-oriented. Note that the approach is successful even though the simple isotropic blurring was unable to produce a perfect grouping and segmentation into individual lines. For instance, one instance of over-merging and many instances of under-merging are evident in the third image representing maximal anisotropy in figure 8. Nevertheless, the compound component orientation computed over the set (typically about a thousand components) is globally consistent with the page alignment.

The third example looks at a sample of 19 images of embryonic tissue taken from Iles

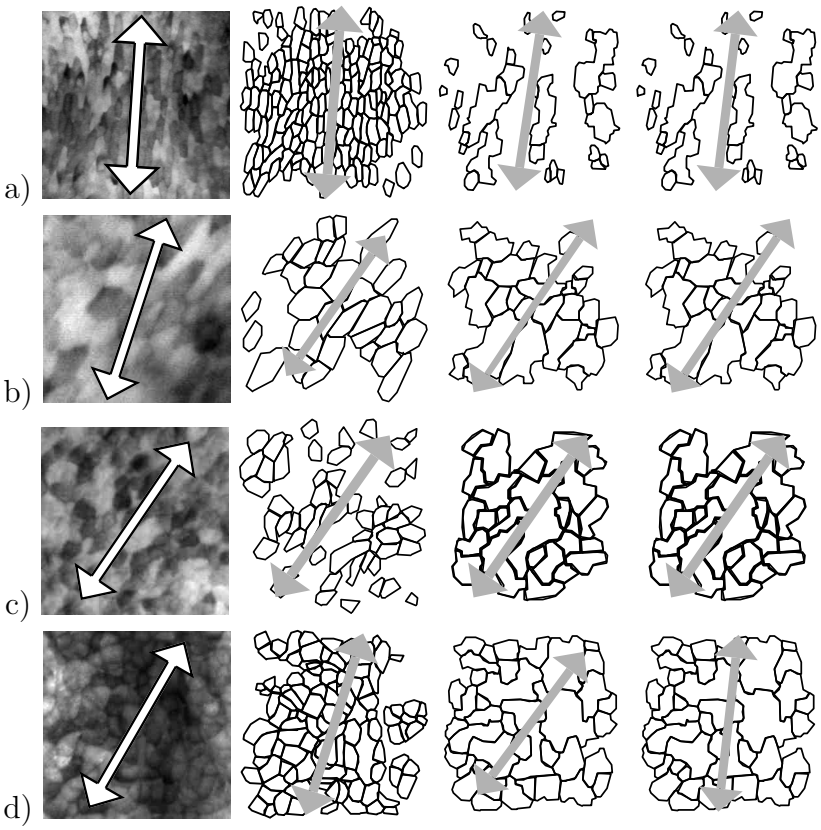

Figure 9: Embryonic tissue. Column 1: original image overlaid with orientation from image tensor. Column 2: ground truth boundaries overlaid with orientation from boundary-based multiple component method. Column 3: watershed algorithm boundaries overlaid with orientation from boundary-based multiple component method. Column 4: watershed algorithm boundaries overlaid with orientation from boundary-based multiple component method applied to line segments.

et al. [10]. The application was to measure the average size, aspect ratio and orientation of the cells since these aspects of cellular fabric are related to the tissue's mechanical properties, and consequently can help develop an understanding of irregularities occurring during morphogenesis that give rise to birth defects.

The image segmentations were taken directly from Iles *et al.* [11] and were obtained by first performing adaptive contrast enhancement and image inversion followed by iterative applications of the extended-minima transform, imposed-minima transform, and watershed segmentation until a target number of segments is found. A final stage removes segments touching the image boundary. Despite the care taken over the segmentation the results are still relatively poor due to the nature of the images, i.e. the inhomogeneity within the images and also across the cells, which often produces low contrast at cell boundaries. For this reason, in addition to the automatically segmented boundaries we also use, for comparison, the ground truth delineation of the main cell outlines provided by Iles *et al.*

In addition to the method proposed in this paper we also compare the popular structure tensor approach [12], in particular the version applied to particle analysis by Scharcanski and Dodson [27]. They compute the covariance (or second moment) matrix

$$C = \begin{bmatrix} I_x^2 & I_{xy} \\ I_{xy} & I_y^2 \end{bmatrix}$$

where I_{xy} is the covariance of the image gradients about the means $\overline{I_x}$ and $\overline{I_y}$. The principal eigenvector of C identifies the dominant orientation, while the eigenvalues of C

$$\begin{aligned} \lambda_{max} &= \frac{I_{xx} + I_{yy} + \sqrt{(I_{xx} - I_{yy})^2 + 4I_{xy}^2}}{2} \\ \lambda_{min} &= \frac{I_{xx} + I_{yy} - \sqrt{(I_{xx} - I_{yy})^2 + 4I_{xy}^2}}{2} \end{aligned}$$

can be used to provide a measure of coherence [12] $\left(\frac{\lambda_{max}-\lambda_{min}}{\lambda_{max}+\lambda_{min}}\right)^2$ or anisotropy [27] $\frac{\lambda_{max}^2}{\lambda_{min}^2}$. These measures are related to the standard moment based region elongation measures, except that region interior pixels are replaced with edge magnitude values over the full image, avoiding the need for segmentation. This should be effective when the objects of interest have good contrast, but problems are to be expected when this is not the case.

The anisotropy measure proposed in this paper was applied to the ground truth boundaries to provide an indication of the degree of orientability of the cell images. Figure 9a and

figure 9b show the two most orientable images, figure 9c shows a cell image with intermediate orientability, while the least orientable image is shown in figure 9d.

The results of the structure tensor approach are overlaid on the original image in the first column, followed in the next column by the results of applying the boundary-based multiple component method to the ground truth regions. The last two columns show results of the boundary-based multiple component method applied to the watershed segmentation boundaries, taking two approaches. The first treats each region boundary as a component, and the second takes individual line segments from the polygonal approximation of the boundaries as separate components. The latter case was considered in case the poor segmentation (in particular the many instances of over-merging) caused problems.

Since the dominant orientation of the cells is so well defined in figure 9a all estimations of the methods are all in agreement despite the poor segmentation. Although figure 9b was also considered to be highly anisotropic (also by the structure tensor approach) the tensor method estimate is inaccurate, perhaps due to the low quality of the image and poor contrast. The boundary-based multiple component method gives the correct result for all the three versions of the data. Similar correct results are also achieved by all methods for the cell image with intermediate anisotropy in figure 9c. Finally, the image in figure 9d is problematic since it has low anisotropy, and so the orientation is ill defined, causing the different methods to produce varying results. Thus we see from these examples that, despite the faulty segmentation, the automatically extracted boundaries contained sufficient information to enable good orientation estimates to be made.

The fourth example is taken from Munich and Perona [22]) who performed identification of (handwritten) signatures. Since the similarity measure used for comparing curves was not invariant to rotation, the curves had to be normalised for orientation before performing matching. They used the standard method (6) which was mostly effective since the signatures tended to be elongated and therefore easily orientable. However, this approach broke down for one subject's signatures which were more compact – see figure 10, top row.

The multiple component method (9) was able to provide a better normalisation. The approach was to segment the curve at vertices with small subtended angles, and then apply the multiple component method to the set of curve segments. To choose an appropriate angle threshold for the segmentation a similar approach was taken to the page deskewing example in figure 8. That is, for each signature the segmentation that maximised the multiple

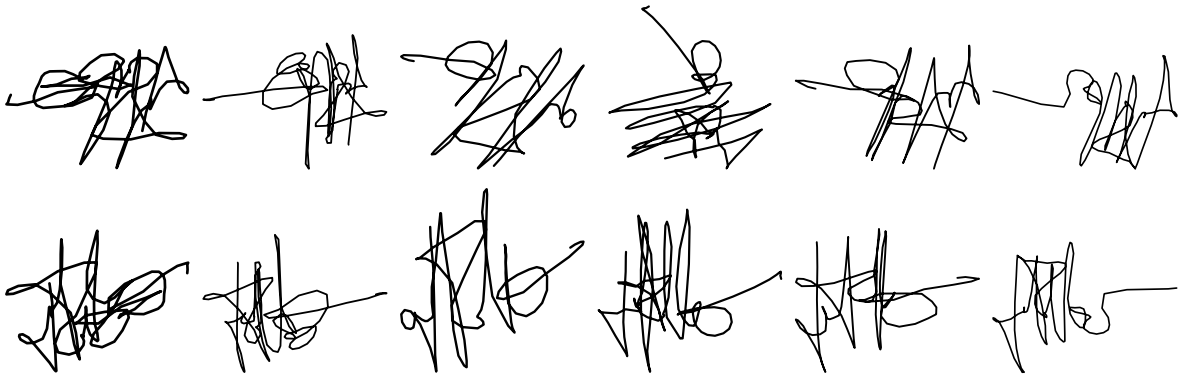

Figure 10: Signatures of subject s048 from Munich and Perona [22]. The top row is re-oriented according to the standard method (6) while the bottom row is re-oriented according to the multiple component method (9).

Figure 11: Signatures of subjects s001, s002, s003, s004 from Munich and Perona re-oriented according to the multiple component method (9).

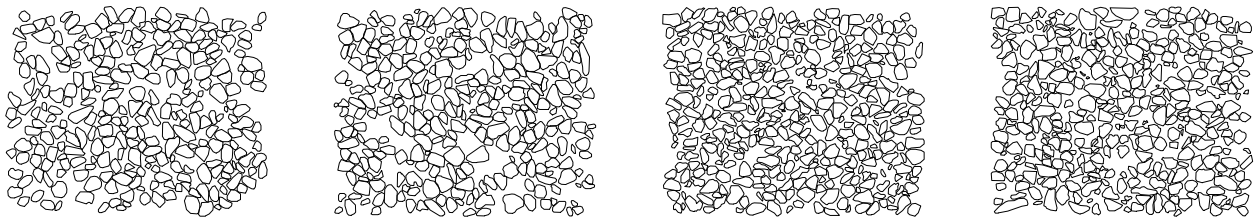

(a) (b) (c) (d)

Figure 12: Examples of boundaries of SEM images of Toyoura sand (Japanese standard sand) prepared using two methods: (a) & (b) moist tamping, (c) & (d) dry deposition.

component anisotropy measure was selected. The results are shown in the bottom row of figure 10. The signatures generally have four or more fairly vertical strokes, which on segmentation provide a good indication of the preferred direction of the signature. A quartic perimeter weighting was used to emphasise the importance of these strokes. Figure 11 demonstrates that when the proposed method is applied in the same manner to other (more easily orientable) signatures it remains effective.

Recently, Yang *et al.* [35] quantified the fabric anisotropy of granular soil in order to investigate its response under applied loading. Such experimental analysis then led to the inclusion of anisotropy in an analytical behaviour model. Our final example describes an application of our approach to the analysis of part of this data. We have 29 samples of the test material (Toyoura sand) – see figure 12 – and these have been prepared using two different methods: 1/ moist tamping (MT) in which sand with 5% water content is laid down in layers and each layer is compacted, and 2/ dry deposition (DD) in which oven dried sand is poured using a funnel. Even under otherwise identical conditions, these different preparations result in different stress responses of the samples under compression. The first step of Yang *et al.* [35] was to characterise the intensity of anisotropy of the preferred particle orientation, and in particular to differentiate between the two preparation methods. To do this they used the "vector magnitude" [5]

$$\Delta = \frac{1}{2N}\sqrt{\left(\sum_{i=1}^{2N}\cos 2\phi_i\right)^2 + \left(\sum_{i=1}^{2N}\sin 2\phi_i\right)^2}$$

where ϕ_i is the orientation of the i'th component. In fact, this is directly related to the circular variance of the directions of the components (orientations are scaled by a factor of two in order to allow for 180° ambiguity).

Although the vector magnitude method was shown to be successful on this data [35] we also show as an alternative that the anisotropy measure proposed in this paper can be applied. Moreover, it has the advantage that it takes into account the size and orientability of the components. Since we do not have a true value of the fabric anisotropy for comparison we test the effectiveness of the anisotropy estimates by performing nearest neighbour classification with leave one out validation. Accuracy with Δ is 62.07%, while our computed anisotropy produced {58.62%, 31.03%, 68.97%} with perimeter weighting set respectively to zero, linear, and quartic. Thus with the last weighting, in which we allow large particles to dominate the measure, a better discrimination between the preparation methods is obtained compared to the "vector magnitude".

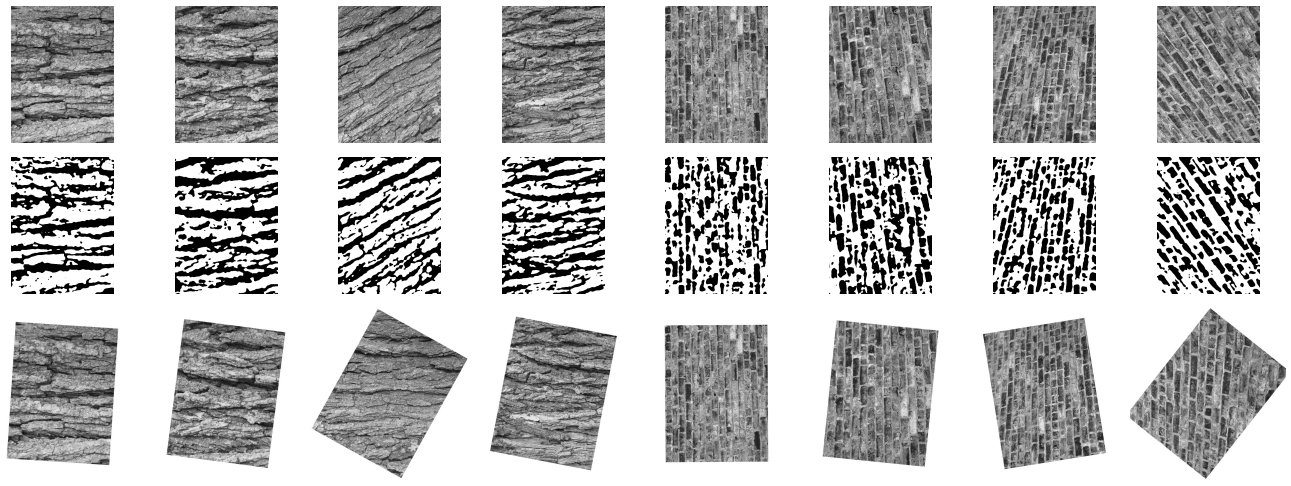

Figure 13: The first 5 images from the tree bark and brick sets before and after orientation normalisation plus the extracted binary regions which make up the multiple component shapes.

	averaged features	directional features
unrotated images	90.72%	84.78%
rotated images	88.91%	**92.56%**

Table 1: Classification rates for UIUC texture database [19] using gray level co-occurrence matrix texture measures.

The final example concerns texture based classification, and uses the database provided

by Lazebnik *et al.* [19], which consists of 25 classes and 40 images per class. Previously [37] we demonstrated that the interior-based multiple component method was capable of reliably computing the texture orientation by first removing global illumination effects, followed by thresholding to extract a set of regions which are treated as a compound shape. The boundary based method presented in this paper produces similar results – see figure 13. In addition, we now use the computed orientation to reorient the images, so that direction specific texture measures can be applied. We have used Haralick *et al.*'s standard texture measures based on the gray level co-occurrence matrix [9][1] The texture measures were calculated separately for four directions. Orientation invariance was obtained either by rotating the image to its canonical orientation, or else by averaging the measures across the four directions.

Following Varma and Zisserman [33], evaluation is performed by performing 1000 random splits of the data, keeping $M = 20$ images per class for training, and testing the classifier on the remaining $40 - M$ images. We use a minimum Mahalanobis distance classifier, and choose an appropriate subset of textures using sequential forward search. As table 1 shows, the classification rate using averaged texture features drops when the rotated images are used rather than the original images. This suggests that the rotation (bilinear interpolation) has degraded the image content. Nevertheless, there is still an overall increase in classification accuracy when the directional texture features are extracted from the rotated images, demonstrating the benefits of our orientation estimation. Classification performance is not as good as the recent results from Varma and Zisserman (97.83%), but are still comparable with the other state of the art accuracies that they report (in the range 90.29%–95.40%).

6 Conclusion

A boundary-based method for computing the orientation α of a shape S has been described. It has the benefit that it leads to a new method for computing the orientation of compound objects which consist of several components. The new method naturally leads to a new measure for shape anisotropy which is a shape descriptor suitable for analysing compound

[1]The gray level co-occurrence matrix was calculated over 7×7 windows with inter-pixel separation of 2, and the following measures extracted: angular second moment, contrast, correlation, variance, inverse difference moment, sum average, sum variance, sum entropy, entropy, difference variance, difference entropy, correlation, recursivity, inverse recursivity. For each image and each measure the measure was averaged over all the 7×7 windows to produce the final texture measure value.

shapes. There are closed formulas for computing both orientation and anisotropy, which enable their simple and efficient computation. Moreover, the new defined anisotropy measure allows the effect of each component on the computed measure to be controlled based on the size of each component and its degree of orientability. The methods are theoretically founded and are experimentally verified by several examples.

The analysis of compound objects requires identifying which components form each object. There are many segmentation and grouping methods that tackle this problem, and so this is not covered here. Moreover, in many applications such as those included in this paper, as well as others in the areas of industrial inspection, biometrics, etc., each image only contains a single multiple component object, avoiding the need for explicit grouping.

As demonstrated in the Introduction, boundary based methods are more sensitive than area based methods to changes in shape that involve small changes in area. This could be considered to be a problem if they are also more sensitive to noise. However, in practise, as shown in the examples in this paper, the effects of noise can be minimised in two ways. The first is straightforward: to perform some noise reduction along the boundary e.g. by carrying out polygonal approximation. The second is that in many applications there will be many components, e.g. the pages of text, cell images, and sand particle images in Section 5. Thus, even if the individual properties from each component have high inherent uncertainties, their combination will tend to produce more reliable estimates of the overall orientation and anisotropy values.

Acknowledgements

We would like to thank: Zhongxuan Yang and Xiang Song Li for providing the mask images for the Toyoura sand SEM data; Peter Iles, David Clausi and Wayne Brodland for providing the embryonic tissue images and segmentation software; and Aditya Vailaya for providing the trademark database.

References

[1] G.P. Arnold. The orientation of plaice larvae (Pleuronectes platessa L.) in water currents. *J. Experimental Biol.*, 50(3):785–801, 1969.

[2] P. Buddharaju, I.T. Pavlidis, P. Tsiamyrtzis, and M. Bazakos. Physiology-based face recognition in the thermal infrared spectrum. *IEEE Trans. on Patt. Anal. and Mach. Intell.*, 29(4):613–626, 2007.

[3] C.-C. Chen. Improved moment invariants for shape discrimination. *Patt. Recog.*, 26(5):683–686, 1993.

[4] D. Coeurjolly and R. Klette. A comparative evaluation of length estimators of digita curves. *IEEE Trans. on Patt. Anal. and Mach. Intell.*, 26(2):252–257, 2004.

[5] J.R. Curray. The analysis of two-dimensional orientation data. *J. Geology*, 64(2):237–248, 1956.

[6] T. Enomae, Y.-H. Han, and A. Isogai. Nondestructive determination of fiber orientation distribution of fiber surface by image analysis. *Nordic Pulp and Paper Research Journal*, 21(2):253–259, 2006.

[7] V. Ferrari, L. Fevrier, F. Jurie, and C. Schmid. Groups of adjacent contour segments for object detection. *IEEE Trans. on Patt. Anal. and Mach. Intell.*, 30(1):36–51, 2008.

[8] V.V. Ganesh and N. Chawla. Effect of particle orientation anisotropy on the tensile behavior of metal matrix composites: experiments and microstructure-based simulation. *Materials Science and Engineering A*, 391(1-2):342–353, 2005.

[9] R. Haralick, K. Shanmugam, and I. Dinstein. Texture features for image classification. *IEEE Trans. on Systems, Man and Cybernetics*, 3(6), 1973.

[10] P.J.W. Iles, G.W. Brodland, D.A. Clausi, and S.M. Puddister. Estimation of cellular fabric in embryonic epithelia. *Computer Methods in Biomechanics and Biomedical Engineering*, 10(1):75–84, 2007.

[11] P.J.W. Iles, D.A. Clausi, and G.W. Brodland. Estimation of average cell shape from digital images of cellular surfaces. In *Computer and Robot Vision*, pages 273–278, 2004.

[12] B. Jähne. *Digital Image Processing*. Springer-Verlag, 2001.

[13] A.K. Jain, Yi Chen, and M. Demirkus. Pores and ridges: High-resolution fingerprint matching using level 3 features. *IEEE Trans. on Patt. Anal. and Mach. Intell.*, 29(1):15–27, 2007.

[14] R. Jain, R. Kasturi, and B.G. Schunck. *Machine Vision*. McGraw-Hill, 1995.

[15] D. Karátson, O. Sztanó, and T. Telbisz. Preferred clast orientation in volcaniclastic mass-flow deposits; application of a new photo-statistical method. *J. Sedimentary Research*, 72(6):823–835, 2002.

[16] R. Klette and A. Rosenfeld. *Digital Geometry*. Morgan Kaufmann, San Francisco, 2004.

[17] R. Klette and J. Žunić. Multigrid convergence of calculated features in image analysis. *J. Math. Imaging Vis.*, 13(3):173–191, 2000.

[18] G. Lambert and H. Gao. Line moments and invariants for real time processing of vectorized contour data. In *Int. Conf. Image Anal. and Proc.*, pages 347–352, 1995.

[19] S. Lazebnik, C. Schmid, and J. Ponce. A sparse texture representation using local affine regions. *IEEE Trans. on Patt. Anal. and Mach. Intell.*, 27(8):1265–1278, 2005.

[20] H. Liu, L.J. Latecki, and W. Liu. A unified curvature definition for regular, polygonal, and digital planar curves. *Int. J. Computer Vision*, 80(1):104–124, 2008.

[21] W. Mio, A. Srivastava, and S. H. Joshi. On shape of plane elastic curves. *Int. J. Computer Vision*, 73(3):307–324, 2007.

[22] M.E. Munich and P. Perona. Visual identification by signature tracking. *IEEE Trans. on Patt. Anal. and Mach. Intell.*, 25(2):200–217, 2003.

[23] T. Pavlidis. A review of algorithms for shape analysis. *Computer Graphics and Image Processing*, 7(2):243–258, 1978.

[24] U. Ramer. An iterative procedure for the polygonal approximation of plane curves. *Computer Graphics and Image Processing*, 1:244–256, 1972.

[25] P.K. Saha and F.W. Wehrli. A robust method for measuring trabecular bone orientation anisotropy at in vivo resolution using tensor scale. *Patt. Recog.*, 37(9):1935–1944, 2004.

[26] C. Samir, A. Srivastava, and M. Daoudi. Three-dimensional face recognition using shapes of facial curves. *IEEE Trans. on Patt. Anal. and Mach. Intell.*, 28(11):1858–1863, 2006.

[27] J. Scharcanski and C.T.J. Dodson. Stochastic texture image estimators for local spatial anisotropy and its variability. *IEEE Trans. Instrumentation and Measurement*, 49(5):971–979, 2000.

[28] L. Schomaker and M. Bulacu. Automatic writer identification using connected-component contours and edge-based features of uppercase western script. *IEEE Trans. on Patt. Anal. and Mach. Intell.*, 26(6):787–798, 2004.

[29] J. Shotton, A. Blake, and R. Cipolla. Multiscale categorical object recognition using contour fragments. *IEEE Trans. on Patt. Anal. and Mach. Intell.*, 30(7):1270–1281, 2008.

[30] N. Sladoje and J. Lindblad. High precision boundary length estimation by utilizing gray-level information. *IEEE Trans. on Patt. Anal. and Mach. Intell.*, 31(2):357–363, 2009.

[31] W.H. Tsai and S.L. Chou. Detection of generalized principal axes in rotationally symmetric shapes. *Patt. Recog.*, 24(1):95–104, 1991.

[32] G. Tzimiropoulos, N. Mitianoudis, and T. Stathaki. A unifying approach to moment-based shape orientation and symmetry classification. *IEEE Trans. on Image Processing*, 18(1):125–1139, 2009.

[33] M. Varma and A. Zisserman. A statistical approach to material classification using image patch exemplars. *IEEE Trans. on Patt. Anal. and Mach. Intell.*, 31(11):2032–2047, 2009.

[34] J. Žunić and M. Stojmenović. Boundary based shape orientation. *Patt. Recog.*, 41(5):1768–1781, 2008.

[35] Z. X. Yang, X. Li, and J. Yang. Quantifying and modelling fabric anisotropy of granular soils. *Géotechnique*, 58(4):237–248, 2008.

[36] J. Žunić, L. Kopanja, and J.E. Fieldsend. Notes on shape orientation where the standard method does not work. *Patt. Recog.*, 39(5):856–865, 2006.

[37] J. Žunić and P.L. Rosin. An alternative approach to computing shape orientation with an application to compound shapes. *Int. J. Computer Vision*, 81(2):138–154, 2009.

[38] J. Žunić, P.L. Rosin, and L. Kopanja. On the orientability of shapes. *IEEE Trans. on Image Processing*, 15(11):3478–3487, 2006.

Appendix A

Proof of Theorem 4. First we show that each function $H(\alpha)$ having the form

$$H(\alpha) = A \cdot \cos(2\alpha) + B \cdot \sin(2\alpha) + C \tag{20}$$

has the minimum and maximum as follows:

$$\max_{\alpha\in[0,2\pi]} H(\alpha) = C + \sqrt{A^2+B^2}, \qquad \min_{\alpha\in[0,2\pi]} H(\alpha) = C - \sqrt{A^2+B^2}. \tag{21}$$

Indeed, if $\alpha = \alpha_0$ is a point where $H(\alpha)$ reaches an extreme value then:

$$\tan(2\alpha_0) = \frac{\sin(2\alpha_0)}{\cos(2\alpha_0)} = \frac{B}{A} \tag{22}$$

follows easily from $\dfrac{dH(\alpha)}{d\alpha} = -2A\sin(2\alpha) + 2B\cos(2\alpha) = 0$. By using (27) and entering the following equalities

$$\sin(2\alpha_0) = \frac{\pm\tan(2\alpha_0)}{\sqrt{1+\tan^2 2\alpha_0}} = \frac{\pm B/A}{\sqrt{1+B^2/A^2}}$$

and

$$\cos(2\alpha_0) = \frac{\pm 1}{\sqrt{1+\tan^2(2\alpha_0)}} = \frac{\pm 1}{\sqrt{1+B^2/A^2}}$$

into (20) we obtain the required $H(\alpha_0) = C \pm \sqrt{A^2+B^2}$ which proves (21).

Further, starting from

$$L_{comp}(\alpha,\partial S) = \sum_{i=1}^{m} \int\int_{\substack{s\in[0,per(S_i)]\\ l\in[0,per(S_i)]}} |\mathbf{pr}_{\overrightarrow{a}}[A_i(s)B_i(l)]|^2 \; ds \; dl \;\; = \;\; \cos^2\alpha \cdot \sum_{i=1}^{m} 2\overline{\mu}_{2,0}(\partial S_i)\cdot\mu_{0,0}(\partial S_i)$$

$$+\sin^2\alpha \cdot \sum_{i=1}^{m} 2\overline{\mu}_{0,2}(\partial S_i)\cdot\mu_{0,0}(\partial S_i) + \sin(2\alpha)\cdot\sum_{i=1}^{m} 2\overline{\mu}_{1,1}(\partial S_i)\cdot\mu_{0,0}(\partial S_i) \tag{23}$$

and by using $\cos^2\alpha = \dfrac{1+\cos(2\alpha)}{2}$ and $\sin^2\alpha = \dfrac{1-\cos(2\alpha)}{2}$ we notice that $L_{comp}(\alpha,\partial S)$ is of the form

$$L(\alpha,\partial S) = A\cdot\cos(2\alpha) + B\cdot\sin(2\alpha) + C$$

where $C = \sum_{i=1}^{m}(\overline{\mu}_{2,0}(\partial S_i) + \overline{\mu}_{0,2}(\partial S_i)\mu_{0,0}(\partial S_i), \quad A = \sum_{i=1}^{m}(\overline{\mu}_{2,0}(\partial S_i) - \overline{\mu}_{0,2}(\partial S_i)\mu_{0,0}(\partial S_i)$ and $B = \sum_{i=1}^{m} 2\overline{\mu}_{1,1}(\partial S_i)\mu_{0,0}(\partial S_i)$.

Finally, by using (21) we obtain the required $\mathcal{A}(S) = \dfrac{C + \sqrt{A^2 + B^2}}{C - \sqrt{A^2 + B^2}}$, where A, B, and C are defined as above. □